

# Dissipation-driven selection under finite diffusion: hints from equilibrium and separation of time-scales

Shiling Liang,<sup>1</sup> Daniel Maria Busiello,<sup>1</sup> and Paolo De Los Rios<sup>1,2</sup>

<sup>1</sup>*Institute of Physics, School of Basic Sciences, École Polytechnique Fédérale de Lausanne - EPFL, Lausanne, 1015, Switzerland*

<sup>2</sup>*Institute of Bioengineering, School of Basic Sciences,  
École Polytechnique Fédérale de Lausanne - EPFL, Lausanne, 1015, Switzerland*

When exposed to a thermal gradient, reaction networks can convert thermal energy into the chemical selection of states that would be unfavourable at equilibrium. The kinetics of reaction paths, and thus how fast they dissipate available energy, might be dominant in dictating the stationary populations of all chemical states out-of-equilibrium. This phenomenology has been theoretically explored mainly in the infinite diffusion limit. Here, we show that the regime in which the diffusion rate is finite, and also slower than some chemical reactions, might give birth to interesting features, as the maximization of selection, or the switch of the selected state at stationarity. We introduce a framework, rooted in a time-scale separation analysis, which is able to capture leading non-equilibrium features using only equilibrium arguments under well-defined conditions. In particular, it is possible to identify fast-dissipation subnetworks of reactions whose Boltzmann equilibrium dominates the steady-state of the entire system as a whole. Finally, we also show that the dissipated heat (and so the entropy production) can be estimated, under some approximations, through the heat capacity of fast-dissipation subnetworks. This work provides a tool to develop an intuitive equilibrium-based grasp on complex non-isothermal reaction networks, which are important paradigms to understand the emergence of complex structures from basic building blocks.

## I. INTRODUCTION

Any chemical system in non-equilibrium conditions with time-independent transition rates will eventually reach a non-equilibrium stationary state [1]. This is maintained at the expenses of a constant energy consumption, and manifests into the presence of steady currents. Predictions stemming from equilibrium arguments about the abundance of chemical species often dramatically fail when there are external sources of energy [2, 3]. Indeed, it has been recently shown that non-equilibrium conditions can trigger stabilization effects in molecular and chemical systems [4–7]. Additionally, the fact that in out-of-equilibrium regimes kinetic aspects are usually as relevant as non-dissipative diffusive properties has been investigated in the last years [8–10].

Recent works [11, 12] have studied the consequences of applying a thermal gradient to a diffusive chemical system. In particular, they elucidated that non-equilibrium conditions couple with an underlying kinetic asymmetry in the transition rates, favouring, at stationarity, a subset of chemical states that are unfavourable at equilibrium [13]. Inspired by the idea that complex high-energy states could have been populated at the dawn of life in non-equilibrium conditions, they refer to this asymmetry in the steady occupation probability of chemical states as selection. Its strength between any two pair of states can be quantified by the unbalance of their steady probabilities. Moreover, this emergent phenomenon is associated with specific features of the stationary energy dissipation into the environment [14]. In a nutshell, non-isothermal conditions allow states that dissipate energy faster, i.e. those participating to the faster reaction pathways and named fast-dissipation states, to be more populated than states with a slower rate of dissipation, at stationarity.

All the presented results about non-equilibrium selection of states are valid in regimes where the Arrhenius law is applicable [1, 15]. Here, we consider again this setting, and the modifications to chemical rates arising from kinetic theory and time-scales analyses lie beyond the subject of this work [16, 17]. However, the major limitation of previous findings on this topic resides in the ideal assumption of a spatial diffusion much faster than all other processes in play, even if they are qualitatively valid even outside this limit.

Here, we explore more realistic cases in which the diffusion coefficient between two thermal reservoirs at different temperatures is finite and the diffusive time-scale is comparable to the one of chemical transition rates [18]. Interestingly, as a function of the diffusion coefficient, the system may experience sharp transitions between phases with different selection strengths. We also find that it is possible to achieve higher selection than in the fast diffusion limit, as well as an inversion in the state that will be selected at stationarity. This complex picture can be captured by a time-scale separation analysis under some approximations, and, as a consequence, we find that appropriate local equilibrium predictions can give precious hints to rephrase and understand these non-equilibrium behaviours.

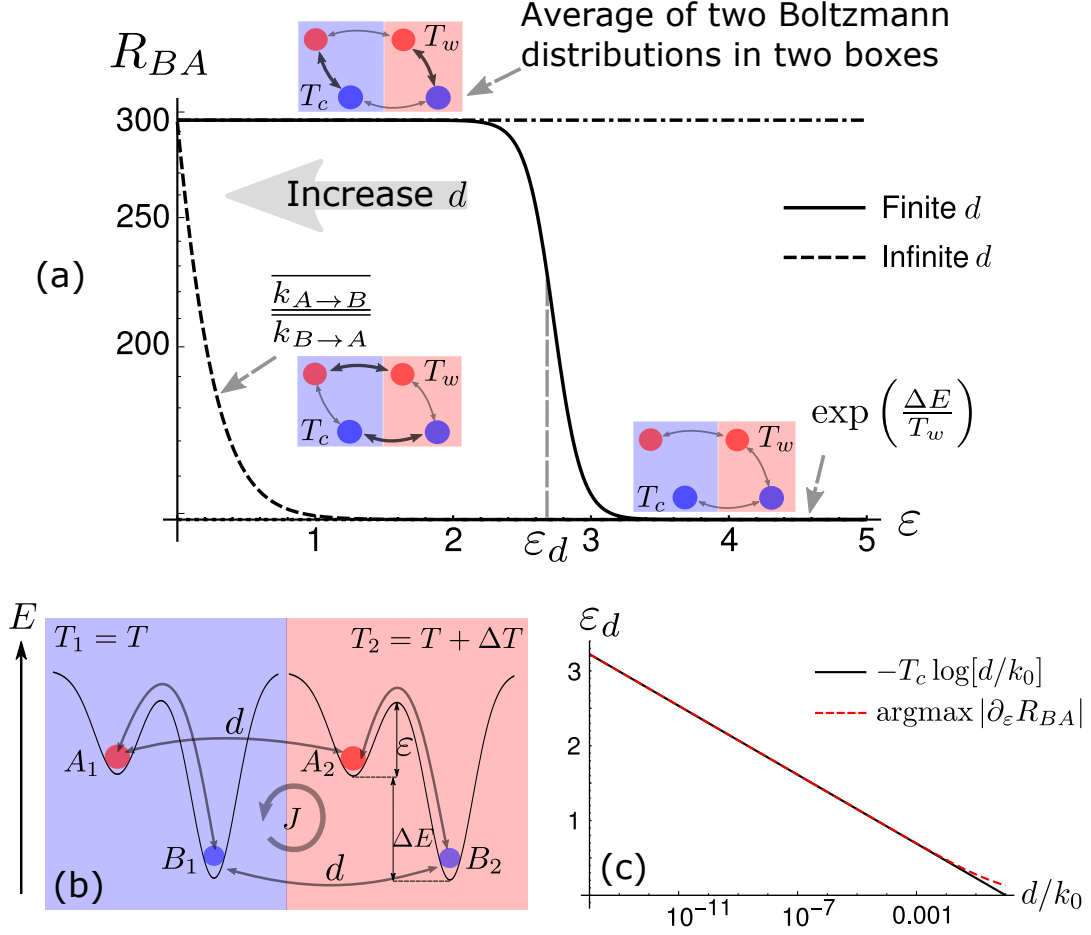


FIG. 1: (a)  $R_{BA} = \overline{P_B}/\overline{P_A}$  as a function of the energetic barrier  $\epsilon$  for both finite and infinite diffusion case. Small insets are sketches of the reaction network in different conditions, where the thickness of the arrows reflects the speed of the corresponding reaction. The solutions in these settings are also reported next to the insets. (b) Sketch of a two-state two-box reaction network in a temperature gradient, where the inner circular arrow represents the direction of non-equilibrium stationary flux  $J$ . (c) The theoretical critical point  $\epsilon_d$  scales linearly with  $d/k_0$ , showing a clear agreement with numerical estimations, with small deviations only for large values of  $d$ .

## II. PHASE-TRANSITION FOR SELECTION IN TWO-STATE SYSTEMS

In order to fix the ideas, let us start considering the simplest case of two chemical species diffusing between two boxes at different temperatures [11]. Being  $P(X_i)$  the time-dependent probability to be in the state  $X$  ( $X = A, B$ ), within the box  $i$  ( $i = 1, 2$ ), where  $i = 1$  indicates the cold box, while  $i = 2$  refers to the hot box. Hence,  $P(X_i)$  satisfies the following reaction-diffusion equations [1]:

$$\begin{aligned} \partial_t P(A_i) &= -k_{B_i A_i} P(A_i) + k_{A_i B_i} P(B_i) + d_A (P(A_j) - P(A_i)) \\ \partial_t P(B_i) &= +k_{B_i A_i} P(A_i) - k_{A_i B_i} P(B_i) + d_B (P(B_j) - P(B_i)) \end{aligned} \quad (1)$$

where  $i = 1, j = 2$  or viceversa, thus the set  $\{A_i, B_i\}_{i=1,2}$  identifies all the possible chemical states of the system in both boxes. Here,  $d_A, d_B$  are the diffusion coefficients of species  $A, B$  respectively, and  $k_{XY}$  indicates the transition rate from state  $Y$  to state  $X$ . When representing a thermally activated transition, as in this case,  $k_{XY}$  has the following Arrhenius form [19–22]:

$$k_{A_i B_i} = k_0 \exp\left(-\frac{\Delta E + \epsilon}{T_i}\right) \quad k_{B_i A_i} = k_0 \exp\left(-\frac{\epsilon}{T_i}\right) \quad (2)$$

where  $T_i$  is the temperature of box  $i$ ,  $\Delta E$  the energy difference between the two chemical states,  $\epsilon$  the energetic barrier, and  $k_0$  a constant pre-factor.

It has been observed [23] that when  $d_A \neq d_B$  thermophoresis [24, 25] can take place, and particles accumulate in one side of the gradient. However, this effect is not detrimental to selection of chemical states, and we consider  $d_A = d_B = d$  throughout the whole manuscript, unless stated otherwise. Moreover, here we consider  $T_1 \equiv T_c < T_2 = T_c + \Delta T \equiv T_w$ . The temperature gradient injects energy into the system, and triggers the onset of a non-equilibrium stationary state. Thermal energy is converted into chemical energy, in the form of an unbalance in state occupancies [11].

In this case, we cannot define a chemical selection, since we have only one low-energy state,  $B$ , hence no kinetic symmetry breaking is possible under non-equilibrium conditions [11], since there could not be any kinetic asymmetry [13]. Indeed, to trigger a selection, the minimal ingredient is the presence of two possible reactions from the high-energy state, one fast and one slow, towards two different low-energy states. Which one of these two will be selected at stationarity is dictated by their kinetics, along with their energies, in out-of-equilibrium conditions [11]. However, in the present case, we consider as a relevant observable the ratio between the total population of the species  $B$ ,  $\overline{P_B} = P(B_1) + P(B_2)$ , and  $A$ ,  $\overline{P_A} = P(A_1) + P(A_2)$ , that is  $R_{BA} = \overline{P_B}/\overline{P_A}$ . From now on, we use the symbol  $\overline{\cdot}$  to indicate the sum of  $\cdot$  in both boxes.

As shown in Fig. 1a, when the transport coefficient  $d$  is finite, we observe a sharp transition in the behaviour of  $R_{BA}$  around a critical barrier,  $\varepsilon_d$ . As  $d$  increases, for any given value of the energetic barrier,  $R_{BA}$  decreases. In the limit of fast diffusion, the transition disappears, hinting at the non-trivial role of finite diffusion in chemical diffusive systems. In order to have an intuitive estimation of  $\varepsilon_d$ , we consider the time-scales of the processes in play. The diffusion is determined by the rate  $d$ , while chemical reactions have their own rates, with the cold box supporting slower reactions. The sharp transition has to happen when these time-scales become comparable. Hence,  $\varepsilon_d$  is defined as the barrier satisfying the following equation:

$$k_0 \exp(-\varepsilon_d/T_c) = d \quad \rightarrow \quad \varepsilon_d = -T_c \ln \frac{d}{k_0} \quad (3)$$

Naively speaking, the slowest downhill transition, i.e. the one in the cold box that populates  $B$ , is equal to the diffusion of  $B$  between boxes, when  $\varepsilon = \varepsilon_d$ . Later on, we will generalize this argument on a more firm ground, based on a time-scale separation procedure. Nevertheless, despite handwaving, the estimate of  $\varepsilon_d$  is compatible with numerical simulations (see Fig. 1c).

As a function of the energetic barrier, we can identify three different behaviors (see Fig. 1a. (i) When  $\varepsilon < \varepsilon_d$ , the system is in the fast-dissipation regime. The system will relax within each box before diffusing, so that the steady state, in this limiting case, is given by the average of two Boltzmann distributions, one at temperature  $T_c$ , the other at temperature  $T_w$  [1]. This is also the maximum possible value for  $R_{BA}$  (see Appendix A). (ii) The transition regime, in which  $\varepsilon \approx \varepsilon_d$ . (iii) The slow-dissipation regime, when  $\varepsilon > \varepsilon_d$ . In this case, all reactions in the cold box are much slower than diffusion, and do not contribute in determining the stationary state. This coincides with the Boltzmann distribution at temperature  $T_w$ . It is evident, even in this simple setting, that equilibrium distributions, along with considerations about interplay among time-scales, might provide useful information about system's behaviors in different genuinely out-of-equilibrium conditions. We also remark that non-equilibrium effects still remain visible in the microscopic fluxes circulating in the system [11, 12]. As shown in Fig. 1b, particles store energy in the hot box, populating  $A$ , then diffuse to the cold side, release heat in the cold box, populating  $B$ , and finally diffuse back to restart the thermal cycle.

We stress that for two-state systems, the infinite diffusion case gives lower values of  $\overline{P_B}/\overline{P_A}$ :

$$\frac{\overline{k_{A \rightarrow B}}}{\overline{k_{B \rightarrow A}}} = \frac{k_{A_1 \rightarrow B_1} + k_{A_2 \rightarrow B_2}}{k_{B_1 \rightarrow A_1} + k_{B_2 \rightarrow A_2}} \quad (4)$$

as already derived in [11].

### III. SIMPLEST CASE FOR SELECTION: A THREE-STATE SYSTEM

Bearing in mind the complex picture described so far, here we investigate a three-state system, which is the simplest case in which it is possible to introduce a kinetic asymmetry, and hence define a selection. Again, we consider the presence of one high-energy state,  $A$ , that can convert into two low-energy states,  $B$  and  $C$ , with the same energy (for the sake of simplicity). The energy barrier between  $A$  and  $B$ ,  $\varepsilon_B$ , is lower than the one between  $A$  and  $C$ ,  $\varepsilon_C$ .  $\Delta\varepsilon = \varepsilon_C - \varepsilon_B$  quantifies the kinetic asymmetry (see Fig. 2a). At equilibrium,  $B$  and  $C$  end up to be equally populated, since they have the same energy. When exposed to a temperature gradient, the system exhibits a selection: the fast-dissipation state,  $C$ , has higher population than the slow-dissipation state  $B$ , in the infinite diffusion limit [11, 12]. The selection parameter is  $R_{CB} = \overline{P_C}/\overline{P_B}$ .

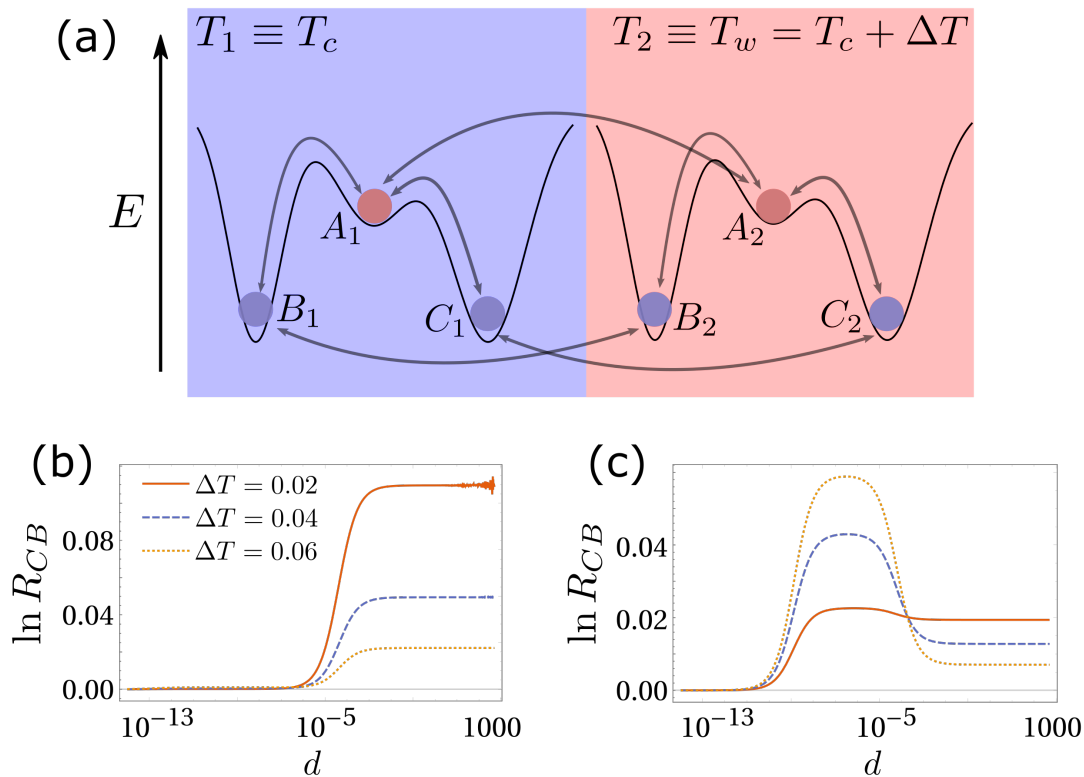


FIG. 2: (a) Three-state two-box reaction network. The same color corresponds to the same value of the energy. The energy difference between  $A$  and  $B$  (or  $C$ ) is  $\Delta E$ . (b)  $\Delta E = 1, T_c = 0.1, \epsilon_C = 1, \epsilon_B = 2$ . We report the logarithm of the selection parameter,  $R_{CB} = \bar{P}_C/\bar{P}_B$ , as a function of  $d$  for different values of the thermal gradient.  $R_{CB}$  is maximized at infinite diffusion. (c) In this case,  $\Delta E = 0.1$ , while all other parameters, and the color-code, are the same as in panel (b). Here, we show a peak in the selection strength for finite diffusion.

Without digging into details about this model, which are extensively reported in [11], we explore what happens when diffusive rate  $d$  is finite. As reported in Fig. 2b-c, the infinite diffusion case does not always lead to the optimal selection. In the numerical example reported in Fig. 2b, reducing the value of  $d$ , the selection reaches a maximum value which is sensibly higher than the one obtained for  $d \rightarrow +\infty$ . However, Fig. 2c reports a situation in which finite  $d$  leads to  $R_{CB}$  lower than the one obtained in the infinite diffusion limit.

Let us understand this picture, following the same reasoning of the previous section. Let us consider the case of Fig. 2b. Here, the energy landscape is nearly flat, i.e.  $\Delta E \ll \epsilon_C, \epsilon_B$ , hence the limiting chemical rates (in the cold box) are dominated by the energetic barrier. When  $d \rightarrow 0$ , all reactions are much faster than diffusion and the system goes back to equilibrium in each box,  $R_{CB} = 0$ . Increasing  $d$ , the reaction between  $A$  and  $B$  in the cold box starts becoming slower than diffusion, while the one between  $A$  and  $C$  stays faster, because of the kinetic asymmetry. Naively speaking,  $C$  equilibrates between both boxes, and the transformation between  $A$  and  $B$  can be ignored for the steady state, resulting in a positive stationary  $R_{CB}$ . Increasing  $d$ , in this case, also the reaction between  $A$  and  $C$  in the cold box becomes slower than diffusion, and the system falls back into the infinite diffusion limit [11, 18, 23]. When the energy landscape is not flat, i.e.  $\Delta E \approx \epsilon_C, \epsilon_B$ , chemical reactions are not governed solely by energetic barriers, and the system is more complicated to analyze on intuitive bases.

Again, we remark that, at least in the case of a nearly flat energy landscape, considerations about time-scales and properly derived equilibrium solutions might improve our understanding of this (slightly more complete) chemical non-equilibrium system.

## IV. TIME-SCALE SEPARATION AND EQUILIBRIUM HINTS

### A. Fast-dissipation chemical subnetworks in two-box models

The time-scale associated with a chemical reaction is the inverse of its corresponding transition rate. This quantity also dictates the dissipation speed along a specific reaction pathway. Analogously, the time-scale associated with diffusion is  $1/d$ , which is also the average occupation time of each box. Intuitively, as discussed above, fast transitions tend to equilibrate the system in their subspace, providing a reliable approximation of the non-equilibrium steady state, employing only equilibrium solutions in fast-dissipation subspaces.

To make these observations quantitative, and to elucidate their limits, we here build a time-scale separation analysis for a generic chemical network [18, 26]. Let us start with the simple case of a nearly-flat energy landscape,  $\Delta E \ll \varepsilon_B, \varepsilon_C$ . In this case, we define two classes of transitions: slow and fast. Slow transitions are associated with the characteristic time  $\tau_S$ , while fast reactions act on the time-scale  $\tau_F$ . Consider, for example, a slow transition from the state  $i$  to  $j$  happening at temperature  $T$ :

$$k_{ji}^S = k_0^S e^{-\frac{\Delta E + \varepsilon_{ij}^S}{T}} \approx k_0^S e^{-\frac{\varepsilon_{ij}^S}{T}} = k_{ij}^S = \kappa_{ij}^S \tau_S^{-1} \quad (5)$$

where  $\kappa_{ij}$  are reaction-specific deviations from a given slow average transition rate  $1/\tau_S$ .

The condition of nearly-flat energy landscape is manifestly crucial to ensure that each transition is slow or fast independently of the direction, i.e.  $\Delta E$  does not play a determinant role. As a consequence, we can split the transition matrix determining the evolution of the system,  $\hat{K}$ , in two parts,  $\hat{K}^S$  and  $\hat{K}^F$ , respectively containing only slow and fast transitions. Indeed, the  $(ij)$ -th element of  $\hat{K}^S$  is  $k_{ji}^S$ , for  $i \neq j$ , while the diagonal elements are  $k_{ii}^S = -\sum_{j \neq i} k_{ij}^S$  in order to have a normalized probability. Further,  $k_{ij}^S$  can be written as in Eq. (5). All these observation holds analogously for  $\hat{K}^F$ .

In a two-box model, as the one described above, we have the following dynamics:

$$\begin{aligned} \partial_\tau P(X_1) = & \sum_{Y_1 \neq X_1} (\kappa_{X_1 Y_1}^S P(Y_1) - \kappa_{Y_1 X_1}^S P(X_1)) + \frac{\tau_S}{\tau_F} \sum_{Z_1 \neq X_1} (\kappa_{X_1 Z_1}^F P(Z_1) - \kappa_{Z_1 X_1}^F P(X_1)) + \\ & + d\tau_S (P(X_2) - P(X_1)) \end{aligned} \quad (6)$$

where  $X, Y, Z = A, B, C, \dots$  indicate the chemical state, while the subscripts 1 and 2 represents the box. A similar equation holds for  $P(X_2)$ . In the model here considered,  $\hat{K}^F$  includes the totality of reactions in the hot box, and only a fraction of them in the cold box. Here,  $\tau = t/\tau_S$  is a slowly evolving a-dimensional time.

First, when  $\tau_F^{-1} > \tau_S^{-1} \gg d$ , the system follows a Boltzmann equilibrium distribution in both the hot and cold box, with temperature  $T_2 \equiv T_w$  and  $T_1 \equiv T_c$  respectively, as for the  $d \rightarrow 0$  case [11, 18]. Indeed, the fast-dissipation subspaces are the chemical reaction networks in each box.

Conversely, the other limiting case already studied in [11, 18] is  $d \gg \tau_F^{-1} > \tau_S^{-1}$ . The system falls back into the fast-diffusion limit, and the stationary state for the total probability is:

$$\lim_{d \rightarrow +\infty} P(X_i) = \frac{1}{2} \Pi^{\text{st}}(X) \quad (7)$$

where  $\Pi^{\text{st}}(X)$  is the stationary distribution of a chemical network with effective rates  $\tilde{k}_{XY} = \overline{k_{XY}}$ , living in one single box. Here,  $\Pi^{\text{st}}(X)$  differs in general from an equilibrium solution, since the effective rates have no longer the Arrhenius form. In this case, the fast-dissipation subnetwork is composed only by diffusive links. Hence, the system first equilibrates in this subspace, reaching a spatial equilibrium distribution, which is uniform in space. Indeed, the numerical factor in Eq. (7) comes from the fact that the probabilities within each box are normalized to  $1/2$  in this regime. Therefore, the population is distributed among chemical states according to an *effective* (a-spatial) equilibrium.

Finally, when  $\tau_F^{-1} \gg d \gg \tau_S^{-1}$ , we are in the richer situation of a finite diffusion regime, with three different time-scales in play. We propose a solution to Eq. (15) of the following form:

$$P(X_i) = P^{(0)}(X_i) + \frac{\tau_F}{\tau_S} P^{(1)}(X_i) \quad (8)$$

Before going on, we remark that fast-dissipative subnetworks are, in general, disconnected sets of chemical reactions,  $S_1, \dots, S_N$ , in the cold box. On the contrary, since  $T_w$  is associated with faster reactions, the whole chemical system

in the hot box is a fast-dissipative subnetwork. Hence, at the zeroth order in  $\tau_F/\tau_S$ , we have a set of disconnected master equations, one for each  $S_i$ , and also a master equation governing the dynamics in the hot box:

$$\begin{aligned} 0 &= \sum_{Y_1^{(i)}} \left( \kappa_{X_1^{(i)} Y_1^{(i)}}^F P^{(0)}(Y_1^{(i)}) - \kappa_{Y_1^{(i)} X_1^{(i)}}^F P^{(0)}(X_1^{(i)}) \right) \quad \forall i = 1, \dots, N \quad \text{subnetworks cold box} \\ 0 &= \sum_{Y_2} \left( \kappa_{X_2 Y_2}^F P^{(0)}(Y_2) - \kappa_{Y_2 X_2}^F P^{(0)}(X_2) \right) \quad \text{whole network hot box.} \end{aligned} \quad (9)$$

In the first line, the superscript  $(i)$  indicates states belonging to the  $i$ -th subnetwork in the cold box.

Eq. (9) is solved by the generic form  $P^{(0)}(X_i) = p(i)\Pi^F(X_i)$ . Here,  $\Pi^F(X_i)$  is the solution for the state  $X_i$ , satisfying the chemical master equation to which  $X_i$  belongs. The prefactor  $p(i)$  depends only on the box considered and it cannot be determined from the zeroth order. Indeed, inserting the expression for  $P^{(0)}$  back, summing over all chemical states, and solving the system up to the first order in  $d\tau_F \gg \tau_F/\tau_S$ , we determine  $p(i)$  by:

$$0 = p(2) - p(1) \quad p(1) = p(2) = 1/2 \quad (10)$$

So that the probability of finding a particle in the box 1 or 2 is equally distributed due to diffusion.

Note that  $P^{(0)}$  satisfies only equilibrium equations at the leading order, since the diffusion enters only in Eq. (10). Hence, equilibrium solutions of fast-dissipative subnetworks are sufficient to provide an accurate approximation of the complete solution in the presence of a net separation of time-scales.

Here the role of the hot box is to excite the chemical reaction network moving particles towards the high energy state. This excitation can also be achieved through other mechanisms, such as photon absorption. One can extract the characteristic time-scales of these excitations, compare them with chemical reaction rates, and build a similar analysis based on fast-dissipation subspaces. Again, reaction networks might be decomposed into fast-dissipation subnets, with the steady-state distribution resulting as a composition of equilibrium distributions of subspaces.

## B. Fast-dissipation ensemble distribution in two-box models

Fast-dissipative subnetworks, however, exhibit interesting ensemble properties that have to be taken into account in order to provide a complete solution to the system in terms of equilibrium distributions.

In fact, considering the first order solution to the full dynamics, and summing over all chemical states constituting each subnetwork,  $(ij) \in S_z$ , and using Eq. (10), we obtain:

$$P(S_i|T_c) = P(S_i|T_w) = \frac{1}{2Z_w} \sum_{z \in S_i} e^{-\frac{E_z}{k_B T_w}} \quad (11)$$

where  $E_z$  is the energy of the state  $z$ ,  $Z_w$  the partition function of the hot box, so that  $P(S_i|T_w)$  is the probability to be in the fast-dissipating set  $S_i$  in the hot box at the leading order. Analogously,  $P(S_i|T_c)$  is the probability of occupation of  $S_i$  in the cold box at the leading order. Note that  $S_i$  is a fast-dissipative subnetwork only in the cold box (see Eq. (9)). Here,  $Z_h$  is a normalization factor. The last equality comes from the fact that high temperature is associated with faster reactions, and then the hot box supports reactions always faster than diffusion in this context. Hence, the ensemble of fast-dissipation subnetworks in the cold box follows a equilibrium-like distribution. Moreover:

$$P(X \in S_i|T_c) = P(S_i|T_c) \frac{1}{Z_c(S_i)} e^{-\frac{E_X}{k_B T_c}} \quad (12)$$

where  $Z_c(S_i)$  is the partition function relative to the subnetwork  $S_i$  in the cold box.

There also exist situations in which the diffusion rate from the cold to the hot box,  $d_{c \rightarrow w}$  is not equal to the reverse one,  $d_{w \rightarrow c}$ , for example for geometrical reasons. In this case:

$$P(S_i|T_c) = \frac{d_{c \rightarrow w}}{d_{w \rightarrow c} + d_{c \rightarrow w}} \frac{1}{Z_w} \sum_{z \in S_i} e^{-\frac{E_z}{k_B T_w}} \quad (13)$$

The interest about these equilibrium-like solutions is twofold: they can provide an intuitive grasp about the interplay between non-equilibrium conditions and selection, and they also can be verified experimentally, without a complete knowledge of the whole system.

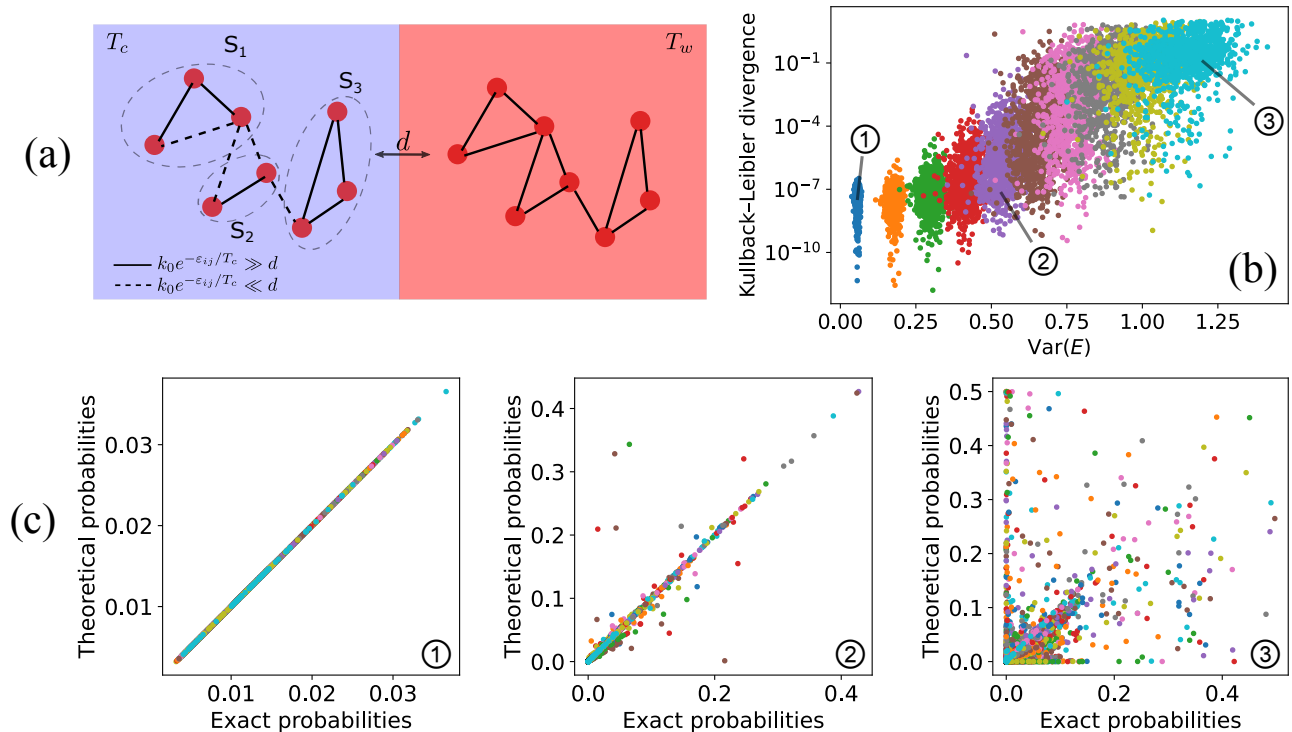


FIG. 3: (a) Two-box model for a complex reaction network. Solid lines represent fast-dissipation reactions, while slow-dissipation reactions are indicated by dashed lines. Gray dashed circles indicate the fast-dissipation subnetworks in the cold box. The distribution inside each subnetwork follows the Boltzmann equilibrium. Overall the probability is redistributed by diffusion, so that half of the total particles populate each box. (b) Theoretical prediction for the stationary probability distribution of reaction networks composed of 40 states, compared with the exact numerical solution. Networks are generated by randomly assigning fast-dissipation ( $\epsilon = 1$ ) and slow-dissipation ( $\epsilon = 5$ ) reactions between states that uniformly populate a given energy range,  $R_E$ . We show the Kullback-Leibler divergence between exact and theoretical solutions, Eq. (14), for  $10^3$  networks in different energy ranges (each one identified by a different color), showing that as the roughness of the landscape increases, the proposed framework starts failing. (c) Theoretical and exact probabilities in comparison for  $R_E = 1, 2$  and  $2.5$  from left to right (different colors represent different networks).

### C. Numerical results and energy landscapes

In Fig. 3a, we report a two-box model for a complex system with nearly-flat energy landscape. Solid lines identify fast-dissipation reactions, whose transition rates are greater than diffusion. Conversely, dashed lines are transitions slower than diffusion, which can be ignored to find the stationary solution at a first-order, as shown above. We also highlight with circles the fast-dissipation subnetworks in the cold box, whose equilibrium solutions (considering only fast reactions) give precious hints about the complete steady-state distribution. It is evident that all reactions in the hot box are marked with solid lines, so that the entire chemical network at temperature  $T_w$  constitutes a fast-dissipation subnetwork. The transition between different regimes is controlled by the value of the diffusion coefficient.

Fig. 3b-c present the agreement between the exact stationary probabilities, obtained numerically integrating the master equation describing the system, and the theoretical predictions stemming from the proposed method, Eq. (12). In particular, in Fig. 3b, we show the Kullback-Leibler divergence ( $K$ ) between exact and theoretical solutions, which acts as a global estimator of their similarity, as a function of the variance of all state energies, an indicator of the roughness of the landscape. Indicating, for the sake of simplicity, with  $P^{\text{exact}}(X)$  and  $P^{\text{theory}}(X)$  respectively the exact and theoretical steady-state probability to be in the state  $X$ , we have:

$$K = \sum_X P^{\text{exact}}(X) \log \frac{P^{\text{exact}}(X)}{P^{\text{theory}}(X)} \quad (14)$$

where the sum runs over all states. Moreover, in Fig. 3c, we present three specific cases of increasing roughness of the

energy landscape, from left to right. For energy landscape flat or not extremely complex (left and central panels), we stress that the agreement is remarkable, even beyond the strict limits of our theoretical derivation, while deviations appear for rough landscapes (right panel). Here, we set only two values for the energetic barriers - one for fast and the other for slow reactions - in order to have a net separation of time-scales, and then we modified the energy landscape. Another possibility, which gives analogous results, is to draw transition rates from a given distribution. Clearly, when there is no net separation of time-scales, our method cannot be straightforwardly applied.

#### D. Fast-dissipation chemical subnetworks for continuous systems

In order to complete the discussion, we here consider the presence of a continuous thermal gradient  $T(x)$ , and describe the system through the probability to be in a given state  $i$ , at a given time  $t$  and position  $x$ ,  $P_i(x, t)$ . In this case, diffusive reactions are replaced by the diffusion Laplacian operator. Clearly, this setting generalizes the two-box model, and the evolution reads:

$$\begin{aligned} \partial_\tau P_i(x, t) = & \sum_{j \neq i} (\kappa_{ij}^S P_j(x, t) - \kappa_{ji}^S P_i(x, t)) + \\ & + \frac{\tau_S}{\tau_F} \sum_{n \neq i} (\kappa_{in}^F P_n(x, t) - \kappa_{ni}^F P_i(x, t)) + D \tau_S \partial_x^2 P_i(x, t) \end{aligned} \quad (15)$$

where  $D$  has the dimension of a diffusion coefficient.

When  $\tau_F^{-1} \gg d \gg \tau_S^{-1}$ , we are in the finite diffusion regime. The main difference with respect to the two-box model is that here we cannot distinguish time-scales of reactions according to the temperature  $T(x)$  at which they happen. In fact, since the temperature varies continuously over the entire domain, subnetworks could be different for each point in space. On the flip side, if some energetic barriers are high enough, so that independently of  $T(x)$  the reactions associated with them will be slower than all the others in play, we can distinguish two different time-scales as before, and consequently identify some fast-dissipation subnetworks. Hence, we propose a solution to Eq. (15):

$$P_i(x, t) = P_i^{(0)}(x, t) + \frac{\tau_F}{\tau_S} P_i^{(1)}(x, t) \quad (16)$$

The resulting zeroth order equations have the following form:

$$0 = \sum_{j \in S_z} (\kappa_{ij}^F(x) P_j^{(0)}(x, t) - \kappa_{ji}^F(x) P_i^{(0)}(x, t)) \quad \forall z = 1, \dots, N, \quad (17)$$

where  $N$  is the number of disconnected subnetworks, as before. The general solution is  $P_i^{(0)}(x, t) = p(x) \Pi_i^F(x)$ , where  $\Pi_i^F(x)$  is the equilibrium solution of the fast chemical subnetwork to which  $i$  belongs. Here,  $p(x)$  encodes spatial variations, and it cannot to be determined from the zeroth order equations. Solving the system up to the first order in  $d\tau_F$ , by summing over all chemical states, we determine  $p(x)$  as the solution of the following diffusive equation:

$$0 = \partial_x^2 P(x) \quad (18)$$

Again, due to diffusion, the solution is homogeneously distributed in space, strengthening the parallel between two-box models and continuous-space systems in this presented framework.

#### V. DIFFUSION-CONTROLLED SWITCH OF SELECTION

Chemical systems, in general, are composed by a set of low-energy states with different energies. Hence, at equilibrium, states are selected according to those, following the Boltzmann distribution. There are situations [12] in which this energetic selection is in competition with the kinetic non-equilibrium selection [13], when fast-reactions do not drive the system towards the lowest energy state.

Since the value of the diffusion coefficient,  $d$ , controls the strength of kinetic (dissipation-driven) selection, the existence of these two competing mechanisms can give birth to a switch of the selected state at stationarity as a function of  $d$ . In Fig. 4, we show this effect for a paradigmatic three-state two-box model. For small  $d$ , i.e.  $d < k_{A \rightarrow B}(T_c)$ , the reactions in both boxes are in local equilibrium, so that the state  $B$  is more populated than  $C$  in the steady-state:

$$P_B = \frac{e^{-E_B/k_B T_c}}{2Z(T_c)} + \frac{e^{-E_B/k_B T_w}}{2Z(T_w)} > \frac{e^{-E_C/k_B T_c}}{2Z(T_c)} + \frac{e^{-E_C/k_B T_w}}{2Z(T_w)} = P_C. \quad (19)$$



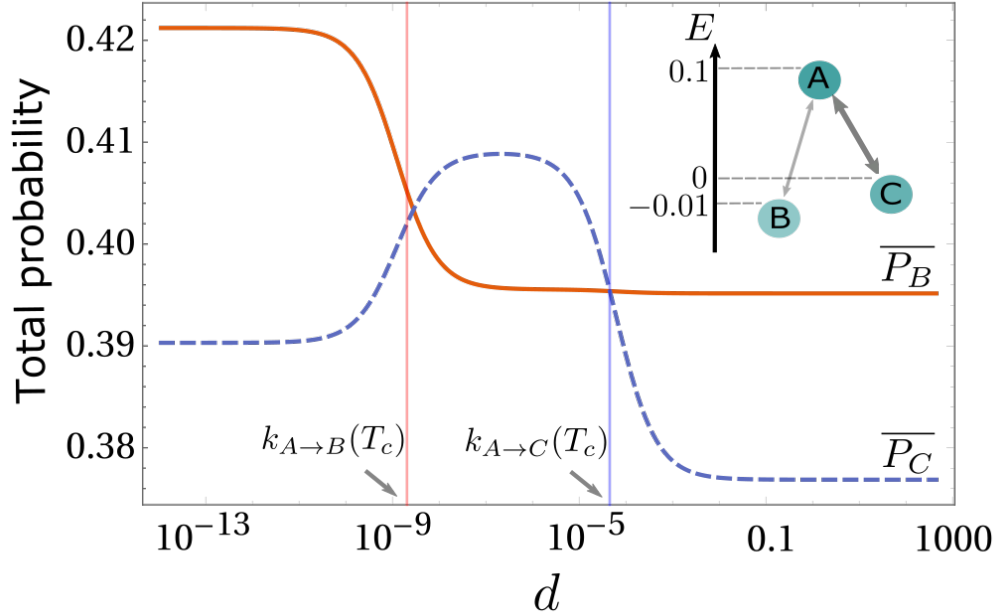


FIG. 4: Total probability of states  $B$ ,  $\overline{P}_B = P(B_1) + P(B_2)$ , and  $C$ ,  $\overline{P}_C = P(C_1) + P(C_2)$ , as a function of  $d$ . The diffusion coefficient can trigger a switch of the selected state at stationarity, which is due to the competition between dissipation-driven and energetic selection. The diffusion coefficients at which each transition happen can be estimated by comparison with the chemical reaction rate in the cold box. The upper inset sketch the chemical network here investigated. Parameters are  $T_c = 0.1$ ,  $T_w = 0.2$ ,  $\varepsilon_C = 1$  and  $\varepsilon_B = 2$ .

When the diffusion coefficient takes intermediate finite values,  $k_{A \rightarrow B}(T_c) = e^{-\varepsilon_B/k_B T_c} < d < k_{A \rightarrow C}(T_c) = e^{-\varepsilon_C/k_B T_c}$ , the transition  $A \rightleftharpoons C$  constitutes a fast-dissipation reaction, while  $A \rightleftharpoons B$  supports slower dissipation. Hence,  $A$  and  $C$  form a fast-dissipation subnetwork reaching local equilibrium in both boxes. However, state  $B$  can not be reached from state  $A$  in the cold box and thus stays in equilibrium with its high-temperature counterpart to which it is connected by diffusion. Here, combining Eq.s (9), (10), and (11),  $P(B)$  and  $P(C)$  are determined by the following equilibrium system:

Equilibrium in the Hot Box (20)

$$\begin{aligned} \dot{P}(A_2) &= -k_{C_2 A_2} P(A_2) + k_{A_2 C_2} P(C_2) - k_{B_2 A_2} P(A_2) + k_{A_2 B_2} P(B_2) = 0 \\ \dot{P}(B_2) &= -k_{A_2 B_2} P(B_2) + k_{B_2 A_2} P(A_2) = 0 \end{aligned}$$

$A \rightleftharpoons C$  equilibrium in the Cold Box (21)

$$\dot{P}(A_1) = -k_{C_1 A_1} P(A_1) + k_{A_1 C_1} P(C_1) = 0$$

Constraints by diffusion (22)

$$\begin{aligned} P(B_1) &= P(B_2) \\ 0.5 &= P(A_1) + P(C_1) + P(B_1) \\ 0.5 &= P(A_2) + P(B_2) + P(C_2) \end{aligned}$$

In the example reported, a strong dissipation-driven selection dominates in this regime (see Fig. 4).

Further increasing  $d$ , all reactions become slower than diffusion and the whole system is effectively dominated by energetic selection in this infinite-diffusion limit:

$$R_{BC} = \frac{\overline{P}_B}{\overline{P}_C} = \frac{\overline{k_{C \rightarrow A}} \overline{k_{A \rightarrow B}}}{\overline{k_{A \rightarrow C}} \overline{k_{B \rightarrow A}}} > 1 \quad (23)$$

The exploration of regimes of finite diffusion, along with the theoretical framework here developed, which is based on equilibrium solutions, might lead to novel phenomena markedly different from those observed in the small- and

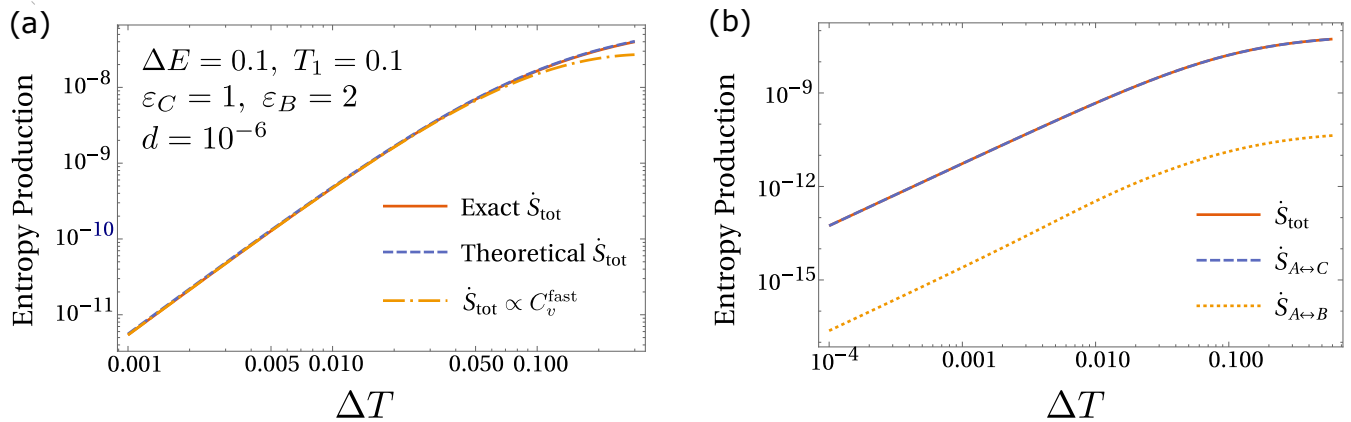


FIG. 5: (a) For a simple three-state system, we compare the exact entropy production (solid red line) with the theoretical approximated one obtained using our framework (blue dashed line), and the formula obtained by a small gradient expansion, Eq. (25) (yellow dot-dashed line). In the exact  $\dot{S}_{\text{tot}}$  the probabilities stem from direct solution of the master equation, while in the theoretical  $\dot{S}_{\text{tot}}$ , and in Eq. (25), the probabilities are obtained employing the equilibration of fast-dissipation subnetworks. To consistently apply our approach, we choose an intermediate value of the diffusion with respect to the chemical rates (see also Fig. 4), showing an excellent agreement among the curves presented. (b) It is evident that the main contribution to the entropy production comes from the reaction  $A \rightleftharpoons C$ ,  $\dot{S}_{A \rightarrow C}$ , which supports a much faster dissipation with respect to the the slow-dissipation branch  $A \rightleftharpoons B$ . Indeed, we also see that  $\dot{S}_{A \rightarrow B} \ll \dot{S}_{A \rightarrow C}$ . Parameters are reported in panel (a).

large-diffusion limit. The existence of a dissipation-controlled switch of selection elucidates this possibility, and this work makes a step towards an *a-priori* understanding of the role of  $d$  with the minimum knowledge of the equilibrium distributions of fast-dissipation subnetworks. Indeed, thermodynamic equilibrium does not depend on energetic barriers, which, in the presented framework, only determine the range of validity of the theoretical predictions.

## VI. EQUILIBRIUM HINTS FOR ENTROPY PRODUCTION

Energy dissipation in discrete-state systems can be quantified using Schnakenberg entropy production,  $\dot{S}_{\text{tot}}$  [14, 22]. This can be divided in two terms, one accounting for the entropy change of the system,  $\dot{S}_{\text{sys}}$ , the other associated with the heat dissipated into the environment,  $\dot{S}_{\text{env}}$ . Since, by definition,  $\dot{S}_{\text{sys}} = (d/dt) (\sum_i P_i \ln P_i)$ , it vanishes in the steady-state. Hence,  $\dot{S}_{\text{tot}} = \dot{S}_{\text{env}}$ , and it also quantifies the heat absorbed by the hot box, or expelled into the cold box. Employing the energy conservation, we have:

$$\dot{S}_{\text{tot}} = \sum_{(ij)} (k_{ij}P_j - k_{ji}P_i) \ln \frac{k_{ij}}{k_{ji}} = d \sum_X E_X (P(X_2) - P(X_1)) \left( \frac{1}{T_1} - \frac{1}{T_2} \right) \quad (24)$$

where the first sum  $\sum_{(ij)}$  runs over all the possible pair of nodes, while the second sum  $\sum_X$  runs over all states in each box. Substituting in Eq. (24) the solutions of the master equation,  $P^{\text{exact}}(X)$  for the state  $X$ , we obtain the exact entropy production (red solid line in Fig. 5a). However, it is possible to estimate energy dissipation in the framework developed so far, by imposing the fast equilibration of fast-dissipation subnetworks. Substituting the steady-state solutions obtained from Eq. (12) in Eq. (24), indicated above as  $P^{\text{theory}}(X)$  for simplicity, we derive an theoretical approximated version of the entropy production which is valid when the diffusion coefficient is in a desired intermediate range (see also Fig. 4). For a simple three-state system, Fig. 5a, we show that the theoretical  $\dot{S}_{\text{tot}}$  (blue dashed line) exhibits an excellent agreement with the exact entropy production.

Moreover, the proposed approach allows us to identify fast-dissipation subnetworks in the cold box, satisfying Boltzmann equilibrium in their subspaces. Hence, it is possible to define, for each of them, the heat capacity,  $C_v^{\text{fast}}(S_i) = \partial_T \langle E \rangle_{S_i}^{\text{fast}}$ , where the average is taken over all the states belonging to  $S_i$ . Again, the fast-dissipation subnetwork in the hot box coincides with the entire chemical network. When  $\Delta T$  is small, the entropy production,

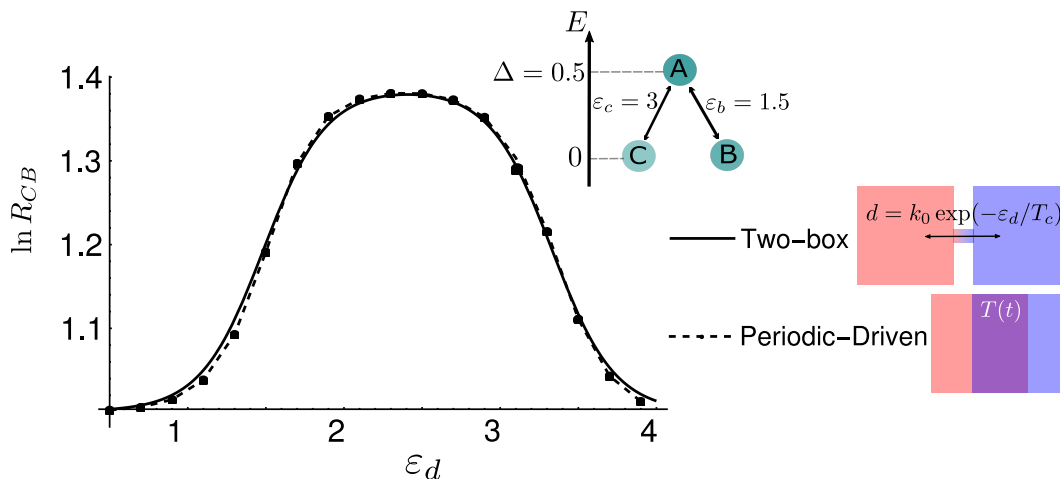


FIG. 6: The logarithm of the selection strength as a function of the critical barrier  $\varepsilon_d$  for a three-state two-box model (solid line), as sketched in the inset, and for a time-periodic driven three-state system (dashed line). These two paradigms are qualitatively and quantitatively equivalent to determine non-isothermal selection of states.

non-zero only out-of-equilibrium, can be expressed in terms of  $C_v^{\text{fast}}(S_i)$ , equilibrium quantities, as follows:

$$\dot{S}_{\text{tot}} \approx d\Delta T \left( \frac{1}{T_1} - \frac{1}{T_2} \right) \sum_i P(S_i|T_c) C_v^{\text{fast}}(S_i) \quad (25)$$

In the expression above,  $P(S_i|T_w)$  does not appear because of the relation in Eq. (11). In Fig. 5a, we compare Eq. (25) (yellow dot-dashed line) with the exact entropy production, reporting an excellent agreement for small  $\Delta T$ .

Additionally, we split the entropy production in the contributions from slow- and fast-dissipation reactions, without using any equilibrium mapping, and we find that the dominant role is played by the reaction path  $A \rightleftharpoons C$ , in accordance with previous results (see Fig. 5b).

## VII. DISCUSSION AND CONCLUSION

Another experimentally feasible way to introduce a temperature gradient is to put the chemical system in contact with a heat bath whose temperature is periodically changed over time. In several conditions, this turns out to be easier than applying a steady thermal gradient [27, 28]. A recent work [11] shows that the time-integrated selection in the time-periodic steady-state can be exactly mapped to the stationary selection for a two-box system. The same equivalence is shown in Fig. 6 in the case of finite diffusion, strengthening the intimate connection between these two frameworks to set the system in out-of-equilibrium conditions.

Summarizing, here we presented a method to deal with complex reaction networks in non-equilibrium conditions triggered by temperature differences. This method is rooted on a time-scale separation analysis, which allows going beyond the infinite diffusion limit and the quasi-equilibrium approximation, capturing behaviours in finite diffusion regime. The power of the proposed approach is that, under some approximations, the genuinely non-equilibrium steady-state can be understood from equilibrium solutions of fast-dissipation subnetworks, which are also accountable for the vast majority of the entropy production in the system.

With this method, we also showed that finite diffusion regime hides numerous intricacies and peculiarities, as a switch of the selected state, or a boost in the selection strength. It would be interesting to push forward the parallel between theoretical idealized systems and experimentally feasible procedures, in order to verify these theoretical predictions. Moreover, observing features of non-isothermal chemistry might also ignite the study of origin of life problems from the point of view of non-equilibrium statistical mechanics and thermodynamics [29–34].

## Acknowledgments

This research was funded by Swiss National Science Foundation, grant 200020\_178763.

- 
- [1] C. Gardiner, *Stochastic methods*, vol. 4 (Springer Berlin, 2009).
  - [2] R. Rao and M. Esposito, *Physical Review X* **6**, 041064 (2016).
  - [3] R. Pascal, A. Pross, and J. D. Sutherland, *Open biology* **3**, 130156 (2013).
  - [4] S. Assenza, A. S. Sassi, R. Kellner, B. Schuler, P. De Los Rios, and A. Barducci, *Elife* **8**, e48491 (2019).
  - [5] P. Goloubinoff, A. S. Sassi, B. Fauvet, A. Barducci, and P. De Los Rios, *Nature chemical biology* **14**, 388 (2018).
  - [6] D. Zwicker, R. Seyboldt, C. A. Weber, A. A. Hyman, and F. Jülicher, *Nature Physics* **13**, 408 (2017).
  - [7] J. M. Horowitz and J. L. England, *Proceedings of the National Academy of Sciences* **114**, 7565 (2017).
  - [8] C. Maes, K. Netočný, and W. O. de Galway, *Journal of Physics A: Mathematical and Theoretical* **47**, 035002 (2013).
  - [9] U. Basu and C. Maes, in *Journal of Physics: Conference Series* (IOP Publishing, 2015), vol. 638, p. 012001.
  - [10] C. Maes, *Non-dissipative effects in nonequilibrium systems* (Springer, 2017).
  - [11] D. M. Busiello, S. Liang, F. Piazza, and P. De Los Rios, *Communications Chemistry* **4**, 1 (2021).
  - [12] A. V. Dass, T. Georgelin, F. Westall, F. Foucher, P. De Los Rios, D. M. Busiello, S. Liang, and F. Piazza, *Nature Communications* **12**, 2749 (2021).
  - [13] R. D. Astumian, *Nature communications* **10**, 1 (2019).
  - [14] J. Schnakenberg, *Reviews of Modern physics* **48**, 571 (1976).
  - [15] P. Hänggi, P. Talkner, and M. Borkovec, *Reviews of modern physics* **62**, 251 (1990).
  - [16] E. Kustova and D. Giordano, *Chemical Physics* **379**, 83 (2011).
  - [17] E. G. Kolesnichenko and Y. E. Gorbachev, *Applied mathematical modelling* **34**, 3778 (2010).
  - [18] D. M. Busiello, D. Gupta, and A. Maritan, *Physical Review Research* **2**, 043257 (2020).
  - [19] I. Klich, O. Raz, O. Hirschberg, and M. Vucelja, *Physical Review X* **9**, 021060 (2019).
  - [20] R. D. Astumian, *Proceedings of the National Academy of Sciences* **104**, 19715 (2007).
  - [21] D. Mandal and C. Jarzynski, *Journal of Statistical Mechanics: Theory and Experiment* **2011**, P10006 (2011).
  - [22] D. M. Busiello, J. Hidalgo, and A. Maritan, *New Journal of Physics* **21**, 073004 (2019).
  - [23] S. Liang, D. M. Busiello, and P. D. L. Rios, arXiv preprint arXiv:2102.03197 (2021).
  - [24] R. Piazza and A. Parola, *Journal of Physics: Condensed Matter* **20**, 153102 (2008).
  - [25] M. Rahman and M. Saghir, *International Journal of Heat and Mass Transfer* **73**, 693 (2014).
  - [26] S. Bo and A. Celani, *Physics reports* **670**, 1 (2017).
  - [27] O. Raz, Y. Subaşı, and C. Jarzynski, *Physical Review X* **6**, 021022 (2016).
  - [28] D. M. Busiello, C. Jarzynski, and O. Raz, *New Journal of Physics* **20**, 093015 (2018).
  - [29] S. Bai, H. Ge, and H. Qian, *Science China Life Sciences* **61**, 1266 (2018).
  - [30] A. Lervik, S. Kjelstrup, and H. Qian, *Physical Chemistry Chemical Physics* **17**, 1317 (2015).
  - [31] X. Jin and H. Ge, *New Journal of Physics* **20**, 043030 (2018).
  - [32] J. L. England, *Nature nanotechnology* **10**, 919 (2015).
  - [33] E. Schrödinger, *What is Life? The Physical Aspect of the Living Cell and Mind* (Cambridge University Press, 1944).
  - [34] I. Prigogine and G. Nicolis, *Quarterly reviews of biophysics* **4**, 107 (1971).

### Appendix A: The maximum possible ratio of two-state system

Let us denote the diffusive flux of a single species in the system as  $J$ . Since there are only two chemical states, the two diffusive fluxes form a cycle with the fluxes due to chemical reactions in both boxes. Since the low energy state is more abundant in the cold box, as discussed in the main text,  $J$  is defined as follows:

$$J = d(P(B_1) - P(B_2)) = -d(P(A_2) - P(A_1)) > 0. \quad (\text{A1})$$

Employing the expression of  $J$ , we can write the steady-state solution of Eq. (1) as:

$$\begin{aligned} P(A_1) &= \frac{k_{A_1 B_1}}{2K_1} + \frac{J}{K_1} & P(B_1) &= \frac{k_{B_1 A_1}}{2K_1} - \frac{J}{K_1} \\ P(A_2) &= \frac{k_{A_2 B_2}}{2K_2} - \frac{J}{K_2} & P(B_2) &= \frac{k_{B_2 A_2}}{2K_2} + \frac{J}{K_2}. \end{aligned} \quad (\text{A2})$$

where  $K_i = k_{A_i B_i} + k_{B_i A_i}$  is the sum of the uphill and downhill rates in the corresponding box,  $i$ . Hence, the ratio between the total probability of finding  $B$  and the total probability of finding  $A$  is:

$$\begin{aligned} R_{BA} &= \frac{\overline{P_B}}{\overline{P_A}} = \frac{P^{eq}(B_1) + P^{eq}(B_2) - J(K_1^{-1} - K_2^{-1})}{P^{eq}(A_1) + P^{eq}(A_2) + J(K_1^{-1} - K_2^{-1})} \\ &\leq \frac{P^{eq}(B_1) + P^{eq}(B_2)}{P^{eq}(A_1) + P^{eq}(A_2)}. \end{aligned} \quad (\text{A3})$$

Note that the box 2 has higher temperature than box 1, thus  $K_1 < K_2$ , and consequently the maximum possible ratio  $R_{BA}$  is obtained in the fast-reaction limit ( $d \ll k_{XY}, \forall X, Y$ ), since  $\lim_{d \ll k_{XY}} J(K_2^{-1} - K_1^{-1}) \rightarrow 0$ .